Journal of Power Sources 195 (2010) 1805–1811

Contents lists available at ScienceDirect

Journal of Power Sources

journal homepage: www.elsevier.com/locate/jpowsour

Noncovalently functionalized graphitic mesoporous carbon as a stable support of Pt nanoparticles for oxygen reduction

Yuyan Shao[a], Sheng Zhang[a], Rong Kou[a], Xiqing Wang[b], Chongmin Wang[a], Sheng Dai[b], Vilayanur Viswanathan[a], Jun Liu[a], Yong Wang[a,*], Yuehe Lin[a,*]

[a] Pacific Northwest National Laboratory, Richland, WA 99352, USA
[b] Oak Ridge National Laboratory, Oak Ridge, TN 37831, USA

ARTICLE INFO

Article history:
Received 14 August 2009
Received in revised form 13 October 2009
Accepted 13 October 2009
Available online 23 October 2009

Keywords:
Graphitized mesoporous carbon
Noncovalent functionalization
Fuel cells
Electrocatalyst
Durability

ABSTRACT

We report a durable electrocatalyst support, highly graphitized mesoporous carbon (GMPC), for oxygen reduction in polymer electrolyte membrane (PEM) fuel cells. GMPC is prepared through graphitizing the self-assembled soft-template mesoporous carbon (MPC) under high temperature. Heat-treatment at 2800 °C greatly improves the degree of graphitization while most of the mesoporous structures and the specific surface area of MPC are retained. GMPC is then noncovalently functionalized with poly(diallyldimethylammonium chloride) (PDDA) and loaded with Pt nanoparticles by reducing Pt precursor (H_2PtCl_6) in ethylene glycol. Pt nanoparticles of ~3.0 nm in diameter are uniformly dispersed on GMPC. Compared to Pt supported on Vulcan XC-72 carbon black (Pt/XC-72), Pt/GMPC exhibits a higher mass activity towards oxygen reduction reaction (ORR) and the mass activity retention (in percentage) is improved by a factor of ~2 after 44 h accelerated degradation test under the potential step (1.4–0.85 V) electrochemical stressing condition which focuses on support corrosion. The enhanced activity and durability of Pt/GMPC are attributed to the graphitic structure of GMPC which is more resistant to corrosion. These findings demonstrate that GMPC is a promising oxygen reduction electrocatalyst support for PEM fuel cells. The approach reported in this work provides a facile, eco-friendly promising strategy for synthesizing stable metal nanoparticles on hydrophobic support materials.

1. Introduction

The polymer electrolyte membrane (PEM) fuel cell is a clean and high-energy-efficiency power source. Even though significant efforts have been made in the research and development of PEM fuel cell and great progresses have been achieved for the past decades, PEM fuel cells are still not commercially available. Currently the most challenging issues to commercialize PEM fuel cells are the prohibitive cost and poor durability [1,2], both of which are heavily dependent on the catalytic electrode materials (typically platinum on carbon support) [1]. Recently, more research efforts have been devoted to improve the durability of PEM fuel cell electrocatalyts [1,2]. The degradation of electrocatalysts generally includes two aspects: carbon support corrosion and catalytic metal (platinum) sintering [2,3]. The corresponding strategies are to develop durable carbon support [4–6] and to alloy Pt with other metals [2,7–14].

Different types of carbons have been developed as PEM fuel cell catalyst supports [4], for example, carbon nanotubes (CNTs) [15–27] and mesoporous carbon (MPC) [28–30]. CNTs with Pt nanoparticles on them have shown enhanced catalytic activity and durability [31,32] compared to the widely used Vulcan XC-72 carbon black due to the specific structures and higher durability of CNTs [33,34]. MPC is another novel carbon with specific pore structures (mainly 2–50 nm of pore sizes) [35–37] which are beneficial for fuel cell application [4,38]. MPC supported Pt or Pt alloys electrocatalysts have shown excellent performances for methanol oxidation [28,29] and oxygen reduction reaction (ORR) [30]. Graphitized carbon nanomaterials [5,39], for example through high-temperature treatment, show promising in improving the electrocatalyst durability, but the challenges remain for loading Pt nanoparticles on them. Usually heat-treatment of porous carbon at high temperatures destroys the pore structures and sharply reduces the specific surface area [40]. In addition, high-temperature annealing removes the structure defects and functional groups of carbon [41] and makes the carbon surface very hydrophobic which is more difficult to uniformly load Pt nanoparticles. Consequently, strong oxidizing acids are used to re-functionalize the graphitized carbon and re-create defects and oxygen functional

* Corresponding authors. Tel.: +1 509 371 6241; fax: +1 509 376 5106.
E-mail addresses: Yongwang@pnl.gov (Y. Wang), Yuehe.lin@pnl.gov (Y. Lin).

0378-7753/$ – see front matter © 2009 Elsevier B.V. All rights reserved.
doi:10.1016/j.jpowsour.2009.10.036

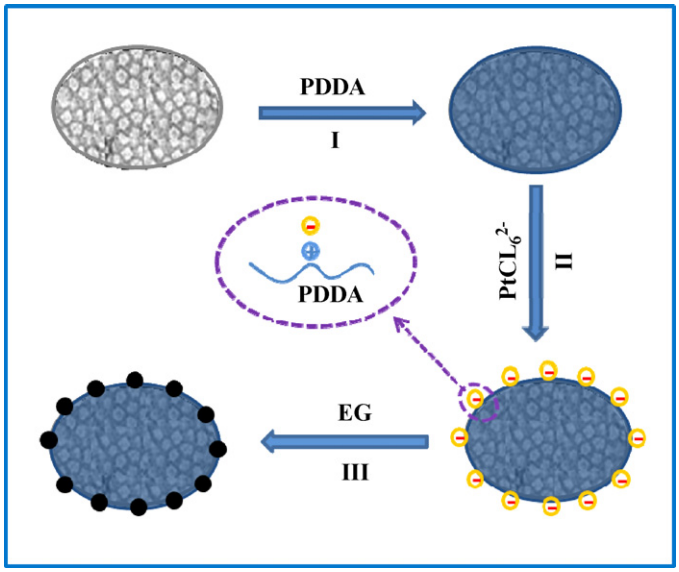

Fig. 1. Schematic of depositing Pt nanoparticles on graphitic mesoporous carbon (GMPC). GMPC is first coated with poly(diallyldimethylammonium chloride) (PDDA), and $[PtCl_6]^{2-}$ is attracted on PDDA/GMPC followed by reduction to Pt nanoparticles in ethylene glycol (EG).

groups before the deposition of Pt nanoparticles [39]. This process is hazardous and not environmentally friendly. The reproduced structural defects will also decrease the electrical conductivity and corrosion resistance of carbon support [42], which reduces the electrocatalytic activity and the durability of electrocatalysts [15]. Therefore, it is necessary to develop a durable graphitized porous carbon with high surface area using an alternative and environmentally friendly strategy to deposit Pt nanoparticles on the carbon support.

The objective of this work is to improve the electrocatalyst durability without losing or even improving activity through materials design and modification. Here, we report a durable electrocatalyst support, highly graphitized mesoporous carbon (GMPC). MPC is synthesized using a self-assembled soft-template method as reported previously [35,43,44] and graphitized at high temperature (2800 °C) to produce GMPC. GMPC is then noncovalently functionalized with a long-chain polyelectrolyte, poly(diallyldimethylammonium chloride) (PDDA) followed by loading Pt nanoparticles (Fig. 1). The mesoporous structure and high specific surface area of MPC are retained using this approach. The synthesis strategies of both mesoporous carbon and Pt/GMPC are facile and effective.

2. Experimental

2.1. Synthesis of graphitic mesoporous carbon

The mesoporous carbon (MPC) was prepared using a self-assembled soft-template method as reported previously [43,44]. In brief, 2.52 g phloroglucinol and 2.52 g polyethyleneoxide-b-polypropyleneoxide-b-polyethyleneoxide (Pluronic F127 $EO_{106}PO_{70}EO_{106}$) were dissolved in 18 g of a mixture of ethanol, water, and 37% HCl with a weight ratio of 10:9:0.1. 2.6 g of 37% formaldehyde solution was then added to the mixture in one batch and stirred for 1 h. A polymer layer was separated from the reactants and cast into a thin film on a 15-cm OD Petri dish. The film was further cured at 80 °C for 12 h after it was dried overnight at room temperature. The cured film was scratched off the Petri dish and carbonized under flowing nitrogen in a tubular furnace, which was ramped to 850 °C at 1 °C min^{-1} and then kept at 850 °C for 2 h. Afterwards, the carbonized sample was heat-treated at 2800 °C for 1 h under helium in a graphite furnace to produce graphitic mesoporous carbon (GMPC). The pores within the GMPCs are tunable in the order of 6–15 nm in diameter. The GMPCs studied here have pores of ~8 nm in diameter. The conductivity of the GMPC is above 300 S cm^{-1}, much higher than that of Vulcan XC-72 carbon (4.0–7.0 S cm^{-1}) [45]. The conductivity of the non-graphitized MPC is only ~2.0 S cm^{-1}.

2.2. Synthesis of Pt/GMPC

First, GMPC was coated with PDDA (MW = 200k–350k, Sigma–Aldrich). Typically, 300 mg GMPC were dispersed in 500 mL 0.5 wt% PDDA aqueous solution and ultrasonicated for at least 3 h to produce a stable dispersion of GMPC. Then the GMPC dispersion was stirred for 24 h. After that, 2.5 g KNO_3 was added to increase the attractive action between PDDA and GMPC surface and lead to a highly functionalized GMPC with PDDA [42,46]. After stirring for another 24 h, the dispersion was filtrated and washed with ultrapure DI water (18.2 MΩ cm, Mill-Q Corp.) to remove the free polyelectrolyte and then dried for 3 h at 90 °C in vacuum.

Next, Pt nanoparticles were loaded onto PDDA-functionalized GMPC by reducing hexachloroplatinic acid (H_2PtCl_6) in ethylene glycol (EG) [15]. Typically, 2.656 mL H_2PtCl_6 EG solution (7.53 mg Pt per mL EG) was added drop by drop into 50 mL EG solution with mechanical stirring for 10 min. NaOH (1 M in EG solution) was added to adjust the pH of solution to above 12. Then 80 mg PDDA-coated GMPC was added to the above solution and stirred for 60 min. The solution was refluxed at 130 °C for 4 h to ensure that H_2PtCl_6 was completely reduced. After cooling down to room temperature and stirring for 12 h, the pH of reaction solution was adjusted to <2 with nitric acid solution (1 M in DI water), which promotes the adsorption of the suspended Pt nanoparticles onto the carbon support, then 20 mL ultrapure DI water was added and stirred for 48 h. The resulting catalyst was washed with ultrapure DI water until no Cl^- was detected and then dried for 3 h at 90 °C in vacuum. A 20 wt% Pt/GMPC electrocatalyst was obtained. A Pt/XC-72 (20 wt% Pt) electrocatalyst was prepared in the same way by depositing Pt nanoparticles on Vulcan XC-72 carbon black.

2.3. Materials characterization

The transmission electron microscope (TEM) images of the catalysts were taken in a JEOL TEM 2010 microscope equipped with an Oxford ISIS system. X-ray diffraction (XRD) patterns in $\theta - 2\theta$ scan mode (0.03° s^{-1}) were obtained using a Philips Xpert X-ray diffractometer using Cu Kα radiation at λ = 1.54 Å. Raman spectra were acquired using a Renishaw inVia Microscope using a 514.5 nm Argon laser at 50% power with a 50× aperture. Nitrogen adsorption/desorption was carried out with a Quantachrome Autosorb 6-B gas sorption system to obtain the BET surface area and BJH pore size distribution.

2.4. Electrochemical tests

The electrochemical tests were controlled with a CHI660C workstation (CH Instruments, Inc., USA). Pt wire and Hg/Hg_2SO_4 (−0.69 V vs. RHE) were used as the counter electrode and reference electrode, respectively. The working electrodes were prepared by applying catalyst ink onto the pre-polished glassy carbon disk electrodes (15 μg Pt/C on 5 mm disk in diameter) [47]. The working electrodes were first activated with cyclic voltammograms (50 mV s^{-1}, 0–1.1 V) in N_2-saturated 0.5 M H_2SO_4 solution until a steady CV was obtained (~100 cycles) in a specially designed 6-channel electrochemical cell (Fig. 2). The durability tests were carried out in N_2-saturated 0.5 M H_2SO_4 solution in the 6-channel

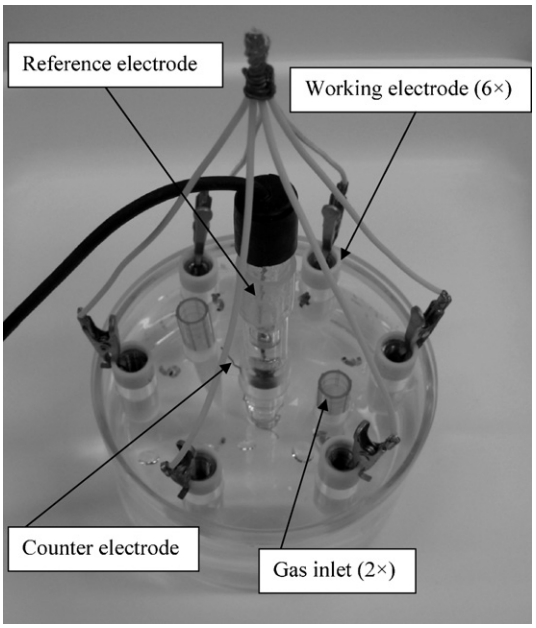

Fig. 2. 6-Channel electrochemical cell (six working electrodes are connected in-parallel).

electrochemical cell with potential step electrochemical stressing method (1.4 V_10 s to 0.85 V_5 s) which focuses on support corrosion [47]. Before and after the degradation test, the linear sweep voltammograms (LSV) for oxygen reduction reaction (ORR) were measured with a rotating disk electrode test system (Pine Instruments Company, USA) in O_2-saturated 0.5 M H_2SO_4 solution (10 mV s^{-1}, 1600 rpm) in a standard 3-electrode cell. All the tests were conducted at room temperature. The electrode potentials were scaled to reversible hydrogen electrode (RHE).

3. Results and discussions

Fig. 3 shows the XRD patterns of MPC and GMPC. It can be seen that three broad XRD diffraction peaks appear on MPC, i.e., C(0 0 2) at $2\theta = 24.0^\circ$, C(1 0 1) at $2\theta = 43.7^\circ$ and a diffraction peak at $2\theta = 79.4^\circ$ [48–50]. For GMPC, the C(0 0 2) ($2\theta = 26.4^\circ$) and C(1 0 1) ($2\theta = 42.8^\circ$) diffraction peaks become sharper and narrower, and several more diffraction peaks become evident, which are assigned to C(0 0 4) at $2\theta = 54.5^\circ$, C(1 1 0) at $2\theta = 77.6^\circ$, C(1 1 2) at $2\theta = 83.5^\circ$, C(0 0 6) at

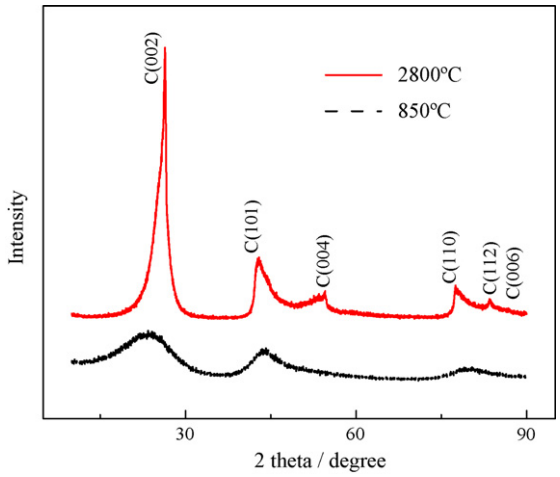

Fig. 3. XRD patterns of MPC (850 °C) and GMPC (2800 °C).

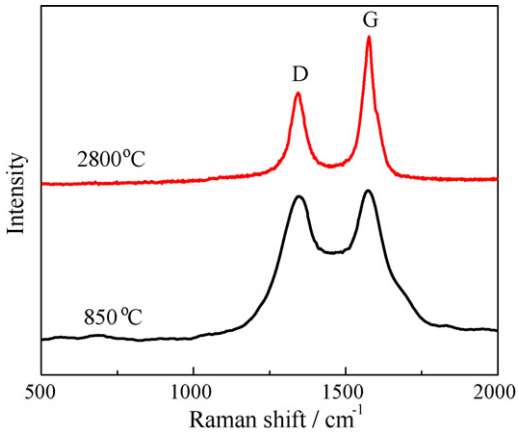

Fig. 4. Raman spectra of MPC (850 °C) and GMPC (2800 °C).

$2\theta = 86.8^\circ$, indicating the high crystallinity (graphitization degree) of the carbon structure in GMPC [5,51]. The interplanar *d*-spacing (d_{002}) can be calculated from the ⟨0 0 2⟩ reflection using Bragg's law ($d = n\lambda/2\sin(\theta)$), which are 3.71 Å and 3.37 Å for MPC and GMPC, respectively. The d_{002} of GMPC is very close to that of an ideal structure of graphite (3.35 Å), which also indicates the highly ordered graphitic structure of GMPC [52].

The Raman spectra of GMPC and MPC are shown in Fig. 4. The two peaks are attributed to the D band at 1340 cm^{-1} and the G band at 1580 cm^{-1}, respectively. The D band is often referred to as the "disordered" band and G band as the "ordered" graphitic band. Therefore, the relative intensity of the G band and D band (I_G/I_D) is indicative of the graphitization degree [5,28]. The I_G/I_D ratio was calculated to be 1.58 and 1.03 for GMPC and MPC, respectively. The higher I_G/I_D ratio of GMPC indicates a much more ordered graphitic structure [53], which is consistent with the XRD results.

Fig. 5 shows the TEM images and the selected area electron diffraction (SAED) pattern of GMPC. The individual layered graphene planes with ribbon-like highly ordered graphitic structures can be observed in the high-resolution TEM image (Fig. 5b). The interlayer distance can be calculated to be 3.37 Å from the SAED pattern. This is consistent with the XRD and Raman analysis.

Fig. 6 shows the nitrogen adsorption/desorption isotherms and the pore size distributions (inset) of mesoporous carbon before and after the heat-treatment at 2800 °C. It can be seen that after the graphitization, the specific surface area decreases from ~500 $m^2\,g^{-1}$ to ~220 $m^2\,g^{-1}$ which is still comparable to that of the widely used Vulcan carbon black XC-72. The reduction of specific surface area is attributed to the elimination of micropores due to the crystallization of the amorphous carbon in MPC. The pore size distribution remains between MPC and GMPC. Therefore, most of the mesoporous structures are retained after high-temperature graphitization while the specific surface area is still sufficiently high for catalyst support application.

Pt nanoparticles were deposited on GMPC and Vulcan carbon XC-72 with the assistance of PDDA. Fig. 7 shows the TEM images of Pt/GMPC and Pt/XC-72. It can be seen that Pt nanoparticles (~3 nm in diameter) are uniformly dispersed on both GMPC and Vulcan carbon XC-72. Generally, it is very difficult to uniformly deposit metal nanoparticles on hydrophobic materials such as GMPC if there is no surface functionalization. But in this work, the long-chain positively charged PDDA [54] can effectively trap the negatively charged $[PtCl_6]^{2-}$ (H_2PtCl_6 was used as a Pt precursor) and help stabilize and disperse Pt nanoparticles on carbon support. Apparently, this PDDA-functionalization strategy allows facile synthesis of Pt nanoparticles on hydrophobic substrates with-

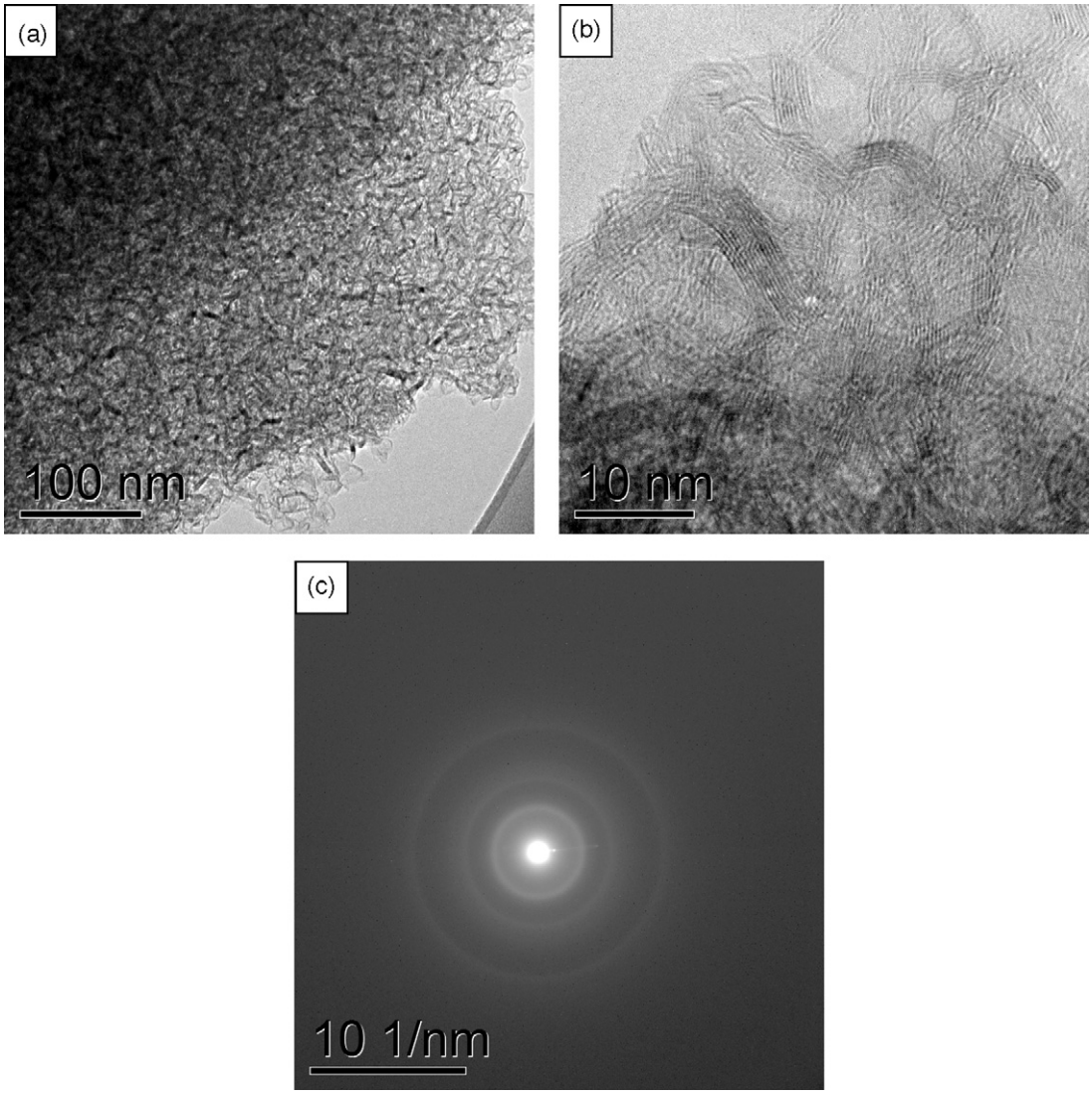

Fig. 5. TEM (a, b) images and the selected area electron diffraction (SAED) (c) pattern of GMPC.

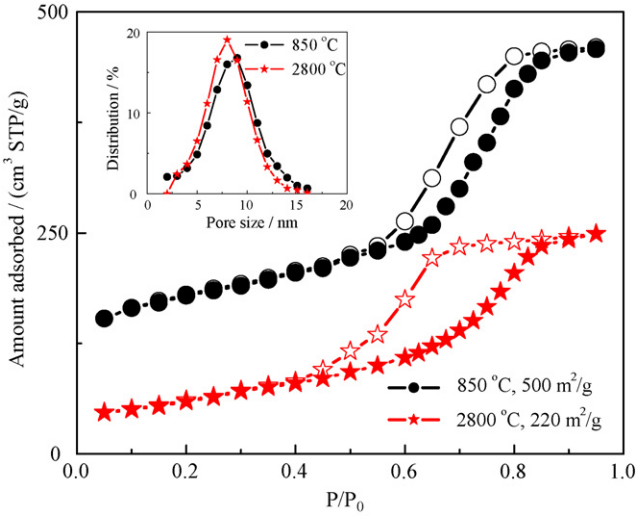

Fig. 6. Nitrogen adsorption/desorption isotherms of MPC (850 °C) and GMPC (2800 °C) (inset: the pore size distributions).

out the concerns of hazardous chemical functionalization processes using strongly oxidizing acids [39,55], which may also destroy the intrinsic structure of graphitic carbon. The facile synthesis method is anticipated to be widely applicable for the synthesis of metal nanoparticles/hydrophobic substrates composites.

Fig. 8 shows the XRD patterns of Pt/GMPC and Pt/XC-72 which reveal the diffraction peaks of both carbon and platinum. The diffraction peaks from graphitic structures of GMPC are still evident and Pt on both samples exhibits similar crystalline structures. Due to the highly graphitic structure of GMPC, Pt and carbon diffraction peaks overlap at around 40° and 82° on Pt/GMPC.

Fig. 9 shows the typical oxygen reduction polarization curves and cyclic voltammograms (CVs, inset) on Pt/GMPC and Pt/XC-72 before and after 44 h electrochemical stressing test. It can be seen that hydrogen adsorption/desorption (0–0.4 V in CVs) are suppressed and the oxygen reduction polarization curves are negatively shifted for both samples. The electrochemical surface areas (ESA) of Pt, which is indicative of Pt nanoparticle dispersion and how many Pt atoms are possibly active in electrochemical reactions, were calculated from the hydrogen adsorption/desorption charge (210 μC cm^{-2}) [56]. The oxygen reduction kinetic currents were obtained using the Koutecky–Levich equation with mass-

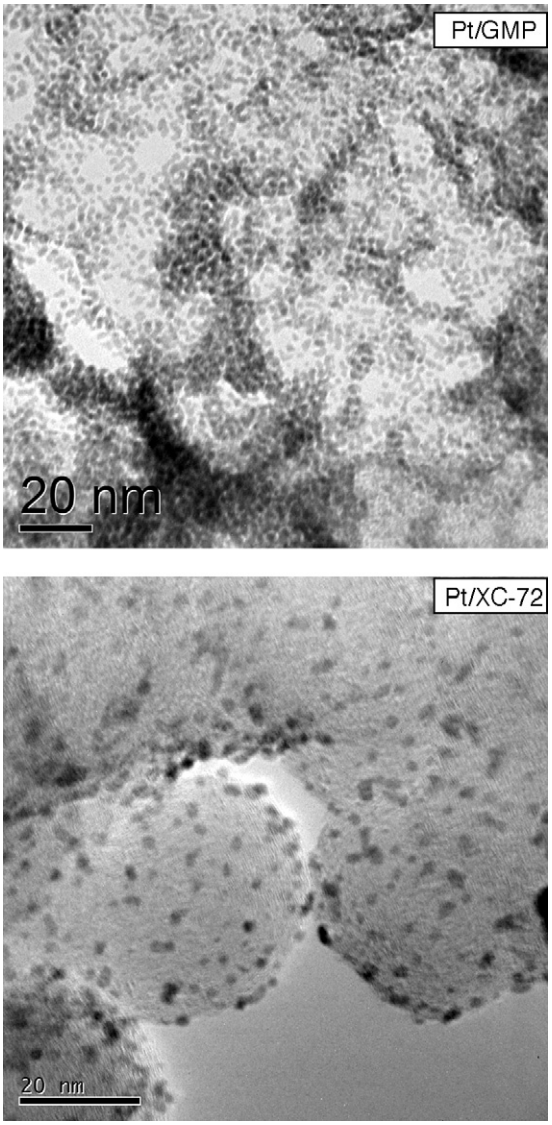

Fig. 7. TEM images Pt/GMPC and Pt/XC-72.

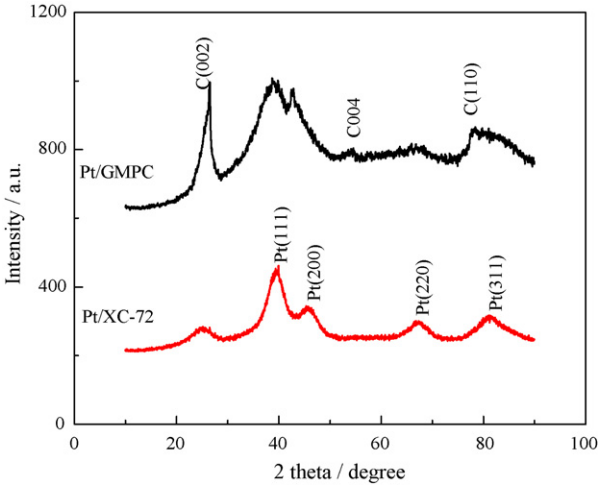

Fig. 8. XRD patterns of Pt/GMPC and Pt/XC-72.

transport correction [11]:

$$I_k = \frac{I_d \times I}{I_d - I} \quad (1)$$

where I_k is the mass transfer-free kinetically controlled ORR current, I_d is the measured diffusion-limited current, and I is the experimentally obtained current (background subtracted). The durability of the electrocatalysts can be characterized by the retention percentages of ESA and ORR values after the electrochemical stressing, which are shown in Fig. 9c and d (we ran three tests for each sample and the data shown here are averaged values with the deviation <±4.0%).

From Fig. 9c, it can be seen that the initial ESA of Pt/GMPC is slightly lower than that of Pt/XC-72, and Pt/GMPC exhibits slightly higher oxygen reduction current density ($A\,g^{-1}$). This might be attributed to the subtle difference in Pt nanoparticle shapes and/or sizes. It might also be due to the difference in the conductivity of supports. GMPC exhibits higher graphitization degree, which usually leads to higher conductivity of carbon materials [4,45,57–59] (>300 $S\,cm^{-1}$ for GMPC vs. 4.0–7.0 $S\,cm^{-1}$ for Vulcan XC-72 [45,58]).

Fig. 9d shows the durability of Pt/GMPC and Pt/XC-72 in terms of the retention percentage of ESA and ORR current density. It can be seen that, after the 44 h electrochemical stressing test, Pt/GMPC retains ~45% of the initial ESA and ORR values but only ~20% of the initial ESA and ORR values for Pt/XC-72. Therefore, the durability of Pt/GMPC is improved by a factor of ~2 under our potential step electrochemical stressing condition which focuses on the degradation of support by separating carbon corrosion from Pt dissolution/redeposition [47]. The durability can also be measured by the degradation in the half-wave potential ($E_{1/2}$) of oxygen reduction [7]. It can be calculated from the oxygen reduction polarization curves (Fig. 9a and b) that the $E_{1/2}$ is negatively shifted by 48 mV and 73 mV for Pt/GMPC and Pt/XC-72, respectively, which indicates that Pt/GMPC is much more durable than Pt/XC-72 [7]. Because the Pt nanoparticle size and crystallinity are similar for both Pt/GMPC and Pt/XC-72 as can be seen from TEM images and XRD patterns, the only key difference between these two electrocatalysts lies in the support materials. More specially, the enhanced durability of Pt/GMPC can be mainly ascribed to the specific properties of GMPC: high degree of graphitization and mesoporous graphitic structures. Following are the general degradation mechanisms of PEM fuel cell electrocatalysts [2,3]: (i) Pt dissolution/redeposition, which is also called the Ostwald ripening process, involves the dissolution of Pt from small particles and the redeposition of soluble Pt species onto large particles, (ii) the migration and coalescence of Pt nanoparticles on the carbon supports, and (iii) the detachment of Pt nanoparticles from carbon supports, which is typically caused by carbon corrosion. We have shown that our accelerated degradation test (ADT) protocol using potential step electrochemical stressing method can separate support corrosion and Pt dissolution/redeposition and the degradation model of Pt/C electrocatalysts under this ADT test is mainly caused by carbon support oxidation [47]. The electrochemical durability of carbon increases with its degree of graphitization [5,31]. This is because the corrosion of carbon usually starts from the structure defects, and carbon with higher degree of graphitization has significantly lower defects [32]. The enhanced π bonding strength of graphene sheets in GMPC due to the increased graphitization degree [60] might make Pt-carbon interaction stronger which also helps stabilize Pt nanoparticles during the degradation test [2,61]. The metal nanoparticle–substrate interactions might be further enhanced by the increased interfacial contact area between the convex metal nanocrystals and concave mesopores in GMPC [61,62]. Therefore, the highly ordered graphitic structures of GMPC contribute to the high durability of Pt/GMPC.

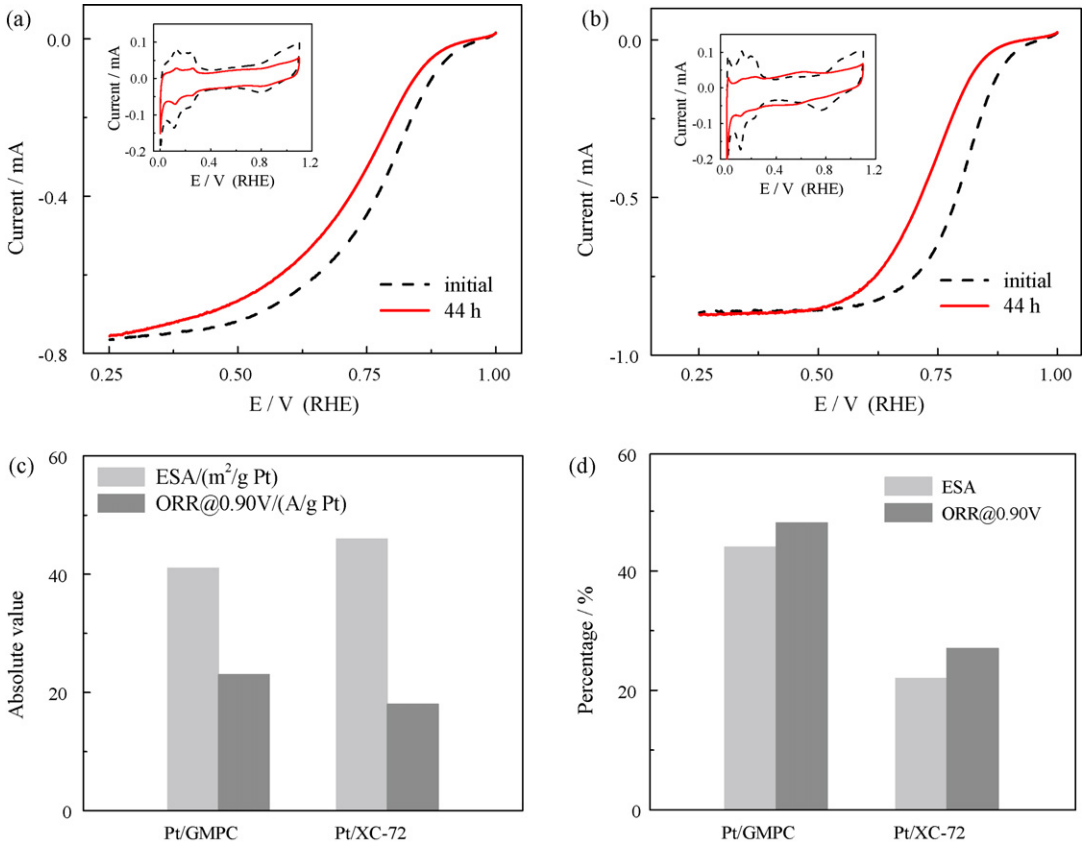

Fig. 9. Linear sweep voltammograms of oxygen reduction (10 mV s^{-1}, 1600 rpm) and cyclic voltammograms (inset, 50 mV s^{-1}) on Pt/GMPC electrode (a) and Pt/XC-72 electrode (b) before and after the degradation test; the initial electrochemical surface areas (ESA) and oxygen reduction kinetic currents (ORR) (c), and the retention percentages of ESA and ORR after the degradation test (d).

4. Conclusions

A highly graphitized mesoporous carbon (GMPC) is prepared by heat treating the self-assembled soft-template mesoporous carbon (MPC) at high temperatures. Pt nanoparticles (~3 nm) are uniformly and facilely deposited on GMPC through the noncovalent functionalization of GMPC with poly(diallyldimethylammonium chloride) (PDDA) followed by reducing Pt precursor in ethylene glycol (EG). Pt/GMPC thus prepared exhibits a much better durability (~2 times) under our potential step electrochemical stressing condition which focuses on support corrosion and higher activity towards oxygen reduction reaction (ORR) than the widely used Pt/XC-72, which are attributed to the enhanced corrosion resistance of graphitic structure of GMPC. GMPC is a promising durable catalyst support for fuel cells. The approach reported here provides a facile and promising strategy to synthesize electrocatalysts with high durability and activity for PEM fuel cells. This strategy can be widely applied to the synthesis of metal nanoparticles on hydrophobic support materials.

Acknowledgment

This work is supported by the U.S. DOE-EERE HFCIT Program. Part of the research described in this paper was performed at the Environmental Molecular Science Laboratory, a national scientific user facility sponsored by DOE's Office of Biological and Environmental Research and located at Pacific Northwest National Laboratory (PNNL). PNNL is operated by Battelle for DOE under Contract DE-AC05-76L01830.

References

[1] R. Borup, J. Meyers, B. Pivovar, Y.S. Kim, R. Mukundan, N. Garland, D. Myers, M. Wilson, F. Garzon, D. Wood, P. Zelenay, K. More, K. Stroh, T. Zawodzinski, J. Boncella, J.E. McGrath, M. Inaba, K. Miyatake, M. Hori, K. Ota, Z. Ogumi, S. Miyata, A. Nishikata, Z. Siroma, Y. Uchimoto, K. Yasuda, K.I. Kimijima, N. Iwashita, Chem. Rev. 107 (2007) 3904–3951.
[2] Y.Y. Shao, G.P. Yin, Y.Z. Gao, J. Power Sources 171 (2007) 558–566.
[3] Y. Shao-Horn, W.C. Sheng, S. Chen, P.J. Ferreira, E.F. Holby, D. Morgan, Top. Catal. 46 (2007) 285–305.
[4] Y. Shao, J. Liu, Y. Wang, Y. Lin, J. Mater. Chem. 19 (2009) 46–59.
[5] P.V. Shanahan, L.B. Xu, C.D. Liang, M. Waje, S. Dai, Y.S. Yan, J. Power Sources 185 (2008) 423–427.
[6] M.K. Debe, A.K. Schmoeckel, G.D. Vernstrorn, R. Atanasoski, J. Power Sources 161 (2006) 1002–1011.
[7] J. Zhang, K. Sasaki, E. Sutter, R.R. Adzic, Science 315 (2007) 220–222.
[8] A.S. Arico, P. Bruce, B. Scrosati, J.M. Tarascon, W. Van Schalkwijk, Nat. Mater. 4 (2005) 366–377.
[9] V.R. Stamenkovic, B.S. Mun, M. Arenz, K.J.J. Mayrhofer, C.A. Lucas, G.F. Wang, P.N. Ross, N.M. Markovic, Nat. Mater. 6 (2007) 241–247.
[10] B. Lim, M.J. Jiang, P.H.C. Camargo, E.C. Cho, J. Tao, X.M. Lu, Y.M. Zhu, Y.A. Xia, Science 324 (2009) 1302–1305.
[11] H.A. Gasteiger, S.S. Kocha, B. Sompalli, F.T. Wagner, Appl. Catal. B-Environ. 56 (2005) 9–35.
[12] H.R. Colon-Mercado, B.N. Popov, J. Power Sources 155 (2006) 253–263.
[13] C.J. Zhong, J. Luo, P.N. Njoki, D. Mott, B. Wanjala, R. Loukrakpam, S. Lim, L. Wang, B. Fang, Z.C. Xu, Energy Environ. Sci. 1 (2008) 454–466.
[14] C.A. Menning, J.G. Chen, J. Chem. Phys. 128 (2008) 164703.
[15] W.Z. Li, C.H. Liang, W.J. Zhou, J.S. Qiu, Z.H. Zhou, G.Q. Sun, Q. Xin, J. Phys. Chem. B 107 (2003) 6292–6299.
[16] X. Sun, R. Li, D. Villers, J.P. Dodelet, S. Desilets, Chem. Phys. Lett. 379 (2003) 99–104.
[17] C. Wang, M. Waje, X. Wang, J.M. Tang, R.C. Haddon, Y.S. Yan, Nano Lett. 4 (2004) 345–348.
[18] Y.H. Lin, X.L. Cui, C. Yen, C.M. Wai, J. Phys. Chem. B 109 (2005) 14410–14415.
[19] Y.L. Yao, Y. Ding, L.S. Ye, X.H. Xia, Carbon 44 (2006) 61–66.
[20] D.J. Guo, H.L. Li, J. Electroanal. Chem. 573 (2004) 197–202.
[21] H. Tang, J.H. Chen, Z.P. Huang, D.Z. Wang, Z.F. Ren, L.H. Nie, Y.F. Kuang, S.Z. Yao, Carbon 42 (2004) 191–197.

[22] A. Kongkanand, S. Kuwabata, G. Girishkumar, P. Kamat, Langmuir 22 (2006) 2392–2396.
[23] Z.D. Wei, C. Yan, Y. Tan, L. Li, C.X. Sun, Z.G. Shao, P.K. Shen, H.W. Dong, J. Phys. Chem. C 112 (2008) 2671–2677.
[24] G. Wu, B.Q. Xu, J. Power Sources 174 (2007) 148–158.
[25] Y.Y. Shao, G.P. Yin, J.J. Wang, Y.Z. Gao, P.F. Shi, J. Power Sources 161 (2006) 47–53.
[26] Y.H. Lin, X.L. Cui, Nanocarbon-based Nanocatalysts: Synthesis and Applications in Fuel Cells, American Scientific Publishers, Stevenson Ranch,CA, 2009.
[27] Y.Y. Shao, R. Kou, J. Wang, C.M. Wang, V. Viswanathan, J. Liu, Y. Wang, Y.H. Lin, J. Nanosci. Nanotechnol. 9 (2009) 5811–5815.
[28] F.B. Su, J.H. Zeng, X.Y. Bao, Y.S. Yu, J.Y. Lee, X.S. Zhao, Chem. Mater. 17 (2005) 3960–3967.
[29] G.W. Zhao, J.P. He, C.X. Zhang, J.H. Zhou, X. Chen, T. Wang, J. Phys. Chem. C 112 (2008) 1028–1033.
[30] Z.H. Wen, J. Liu, J.H. Li, Adv. Mater. 20 (2008) 743–747.
[31] X. Wang, W.Z. Li, Z.W. Chen, M. Waje, Y.S. Yan, J. Power Sources 158 (2006) 154–159.
[32] Y.Y. Shao, G.P. Yin, Y.Z. Gao, P.F. Shi, J. Electrochem. Soc. 153 (2006) A1093–A1097.
[33] L. Li, Y.C. Xing, J. Electrochem. Soc. 153 (2006) A1823–A1828.
[34] Y.Y. Shao, G.P. Yin, J. Zhang, Y.Z. Gao, Electrochim. Acta 51 (2006) 5853–5857.
[35] C.D. Liang, Z.J. Li, S. Dai, Angew. Chem. Int. Ed. 47 (2008) 3696–3717.
[36] A. Stein, Z.Y. Wang, M.A. Fierke, Adv. Mater. 21 (2009) 265–293.
[37] J. Lee, J. Kim, T. Hyeon, Adv. Mater. 18 (2006) 2073–2094.
[38] K.Y. Chan, J. Ding, J.W. Ren, S.A. Cheng, K.Y. Tsang, J. Mater. Chem. 14 (2004) 505–516.
[39] J.J. Wang, G.P. Yin, Y.Y. Shao, Z.B. Wang, Y.Z. Gao, J. Phys. Chem. C 112 (2008) 5784–5789.
[40] D.A. Stevens, M.T. Hicks, G.M. Haugen, J.R. Dahn, J. Electrochem. Soc. 152 (2005) A2309–A2315.
[41] D. Bom, R. Andrews, D. Jacques, J. Anthony, B.L. Chen, M.S. Meier, J.P. Selegue, Nano Lett. 2 (2002) 615–619.
[42] S. Wang, S.P. Jiang, X. Wang, Nanotechnology 19 (2008) 265601.
[43] C.D. Liang, S. Dai, J. Am. Chem. Soc. 128 (2006) 5316–5317.
[44] X.Q. Wang, C.D. Liang, S. Dai, Langmuir 24 (2008) 7500–7505.
[45] D. Pantea, H. Darmstadt, S. Kaliaguine, L. Summchen, C. Roy, Carbon 39 (2001) 1147–1158.
[46] J. Park, P.T. Hammond, Macromolecules 38 (2005) 10542–10550.
[47] Y.Y. Shao, R. Kou, J. Wang, V.V. Viswanathan, J.H. Kwak, J. Liu, Y. Wang, Y.H. Lin, J. Power Sources 185 (2008) 280–286.
[48] R. Andrews, D. Jacques, D. Qian, E.C. Dickey, Carbon 39 (2001) 1681–1687.
[49] N. Iwashita, C.R. Park, H. Fujimoto, M. Shiraishi, M. Inagaki, Carbon 42 (2004) 701–714.
[50] Z.Q. Li, C.J. Lu, Z.P. Xia, Y. Zhou, Z. Luo, Carbon 45 (2007) 1686–1695.
[51] T.W. Kim, I.S. Park, R. Ryoo, Angew. Chem. Int. Ed. 42 (2003) 4375–4379.
[52] C.D. Liang, S. Dai, G. Guiochon, Anal. Chem. 75 (2003) 4904–4912.
[53] F. Tuinstra, J.L. Koenig, J. Chem. Phys. 53 (1970) 1126–1130.
[54] S.P. Jiang, Z.C. Liu, H.L. Tang, M. Pan, Electrochim. Acta 51 (2006) 5721–5730.
[55] Y.C. Xing, J. Phys. Chem. B 108 (2004) 19255–19259.
[56] Y.Y. Shao, G.P. Yin, J.J. Wang, Y.Z. Gao, P.F. Shi, J. Electrochem. Soc. 153 (2006) A1261–A1265.
[57] A.B. Fuertes, S. Alvarez, Carbon 42 (2004) 3049–3055.
[58] D. Pantea, H. Darmstadt, S. Kaliaguine, C. Roy, Appl. Surf. Sci. 217 (2003) 181–193.
[59] F. Coloma, A. Sepulvedaescribano, F. Rodriguezreinoso, J. Catal. 154 (1995) 299–305.
[60] F. Coloma, A. Sepulvedaescribano, J.L.G. Fierro, F. Rodriguezreinoso, Langmuir 10 (1994) 750–755.
[61] G. Gupta, D.A. Slanac, P. Kumar, J.D. Wiggins-Camacho, X.Q. Wang, S. Swinnea, K.L. More, S. Dai, K.J. Stevenson, K.P. Johnston, Chem. Mater. 21 (2009) 4515–4526.
[62] G. Gupta, M.N. Patel, D. Ferrer, A.T. Heitsch, B.A. Korgel, M. Jose-Yacaman, K.P. Johnston, Chem. Mater. 20 (2008) 5005–5015.